COMMUNICATION

Stability Assessment on a 3% Bilayer PbS/ZnO Quantum Dot Heterojunction Solar Cell

By *Joseph M. Luther,* Jianbo Gao, Matthew T. Lloyd, Octavi E. Semonin, Matthew C. Beard,* and *Arthur J. Nozik*

The performance of thin film optoelectronic devices comprised of lead chalcogenide (PbX) quantum dots (QDs) has seen rapid development since 2005. Lead chalcogenides have uniquely large dielectric constants and therefore large exciton Bohr radii that result in a significant degree of quantum confinement.[1] For example, PbX QDs are easily synthesized with band gaps ranging from 0.5 to 2.0 eV.[2–5] Such large Bohr Radii (18 and 47 nm for PbS and PbSe) and small effective masses for electrons and holes (~0.09 m_e) promote charge delocalization in QD films giving rise to an increase in charge carrier mobility and thus the conductivity. Field effect transistors in which current flows laterally, controlled by a gate bias, through a PbSe QD film on a Si wafer brought increased attention to PbX QD films. Soaking the film in hydrazine allows for an *n*-type gated response and control over the majority carrier type was demonstrated by thermal treatment which removes volatile hydrazine molecules resulting in *p*-type behavior.[6] Subsequently, Wang *et al.* directly demonstrated carrier type inversion in similar QD films through thermopower measurements.[7] In addition to short-chained amines like hydrazine and also butylamine,[8] simple thiol-terminated molecules aggressively remove the native oleate ligand, and allow for strong electronic coupling in QD arrays.[9–11] Along these lines, 1,2-ethanedithiol (EDT) has received considerable attention in coupled films of PbS and PbSe QDs. 1,4- and 1,3-benzenedithiol work similarly well and have been reported to increase the air stability of films due to reduced volatility compared to hydrazine or EDT.[12,13] Additional studies of the structural, optical and electrical properties of coupled arrays of PbSe and PbS using a variety of thiols, amines, and acids have been reported.[10,14,15]

From a materials standpoint, Wadia *et al.* has identified PbS as an abundant, inexpensive semiconductor material that is capable of supplying enough annual electricity to meet global demand, however it is limited by having a bulk band gap (0.41 eV) too low for general acceptance as a photovoltaic material.[16] By adding quantum confinement, the band gap can be tuned to 1–1.4 eV, thereby falling in the range that best optimizes electrical conversion of the solar spectrum.

Photovoltaic cells incorporating QDs of PbS, PbSe, and their alloy, PbSSe, were first constructed with a simple back-contact Schottky junction between a *p*-type QD film and a low work function metal electrode.[9,11–13] Depositing the QD film onto ITO forms an ohmic contact and evaporating a metal with a low work function, such as Ca, Mg, or Al, forms the Schottky contact. Often, Schottky-junction PV cells suffer from low built-in voltages, thus limiting their power conversion efficiency. Several reports followed that employ *n*-type materials which form a heterojunction with the *p*-type QD film. ZnO, amorphous-Si, and C_{60} have been paired with PbS and PbSe to form heterojunctions.[17–21] Choi *et al.* showed that ZnO nanocrystals (NCs) can be spin coated on top of a PbSe film prior to deposition of the evaporated metal contact.[17] The NC ZnO layer helps to increase the voltage by creating a pseudo p-n junction, since PbSe QD films treated with thiols show *p*-type behavior under illumination,[10] and ZnO is a well-known *n*-type material. Leschkies *et al.* has shown ZnO/PbSe heterojunction devices where the ZnO is deposited below the QD film.[18,19] The size-dependent energetics between PbX QDs and various other materials including ZnO are reported by the groups at Cornell.[17,22]

Placing ZnO under the PbSe film inverts the polarity of the device when a high work function metal is deposited on top of the QD layer. A similar geometry employed in the organic photovoltaic (OPV) community is termed an 'inverted cell' because electrons flow toward the substrate rather than the evaporated metal contact, thus creating an inverted polarity.[23] For PbX QD solar cells, an inverted geometry advantageously locates the depletion region adjacent to the ITO, allowing the use of thicker films necessary for increased light absorption yet without compromising the utilization of high energy photons.[24] Leschkies *et al.* demonstrated that when ZnO nanowires penetrate into the PbSe QD film, 600 nm thick films could be used because the effective junction is extended throughout the film.[19] The inverted geometry allows for more stable contacts such as Au to be used vs. Ca, Mg or Al, which readily oxidize.

Tang *et al.* recently developed PbS QDs that exhibit high air stability.[25] When a film of ~1.1–1.3 eV (3.5–5.2 nm) PbS QDs is deposited in air rather than in a glove box the devices exhibit increased stability in air. The authors employ LiF/Al/Ag as the low work function contact in a Schottky cell and demonstrate devices with enhanced stability compared to those with other contacts such as Ag or Al without LiF.[26]

[*] J. M. Luther, J. Gao, M. T. Lloyd, O. E. Semonin, M. C. Beard, Prof. A. J. Nozik
National Renewable Energy Laboratory
1617 Cole Blvd., Golden CO, 80401 (USA)
E-mail: joey.luther@nrel.gov
J. Gao
University of Toledo
Toledo, OH, 43606 (USA)
O. E. Semonin, Prof. A. J. Nozik
University of Colorado
Boulder, CO, 80309 (USA)

DOI: 10.1002/adma.201001148

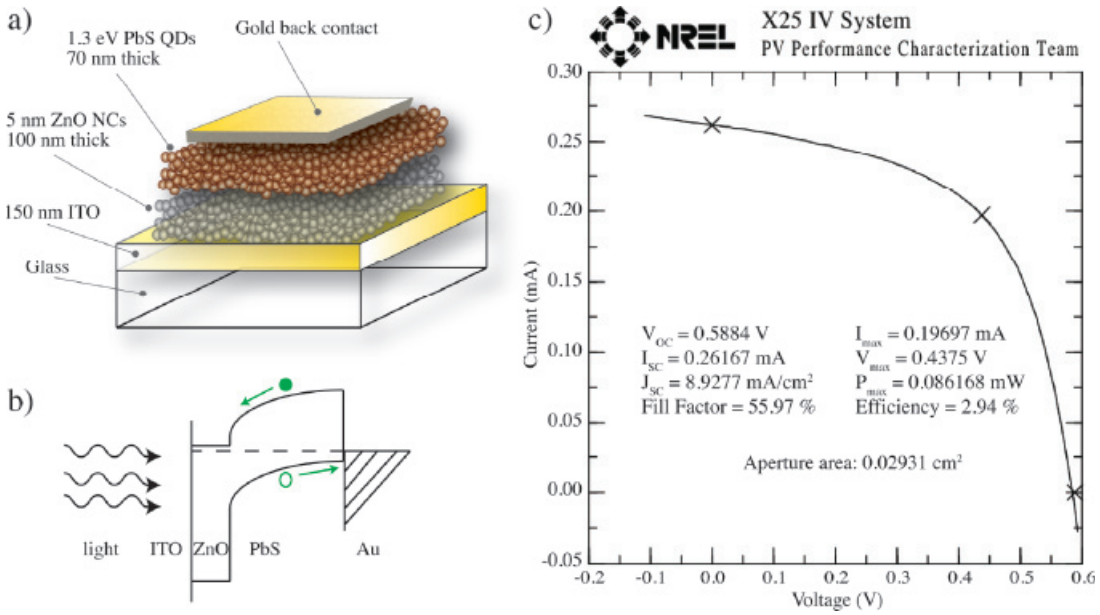

Figure 1. a) Depiction of the device structure used in this work. Light is incident through the glass. b) Proposed band diagram for the operation of the solar cell. c) Measured IV characteristics for ZnO/PbS nanocrystal heterojunction device. A copper aperture was placed over a 0.11 cm^2 area device so as to prevent photocurrent generated outside the active area of the cell. Various device parameters are listed in the inset.

Here we constructed a cell composed of ZnO NCs similar to Choi *et al.*,[17] in an inverted geometry similar to Leschkies *et al.*,[18] using air stable 1.3 eV PbS QDs as described by Tang *et al.*[25] We used Au as the top contact without additional electron blocking layers. **Figure 1** shows a schematic of the device architecture along with the energy band diagram at equilibrium.

After three days of storage in air, the device was submitted to the NREL measurements and characterization group for an official measurement of the AM1.5G 1-sun efficiency, η, calculated by

$$\eta = \frac{V_{OC} \times I_{SC} \times FF \times M}{A \times P_{IN}} \quad (1)$$

where V_{OC} is the voltage at open circuit, I_{SC} is the current at short circuit, FF is the maximum power divided by the $V_{OC} \times I_{SC}$ product, M is the spectral mismatch, A is the illuminated device area, and P_{IN} is the incident optical power density (1000 W m^{-2}). The spectral mismatch depends on the light source, reference solar cell, the spectral response of the device under test and the actual solar spectrum.[27]

Figure 1c shows the light IV curve for the masked area device using the X25 solar simulator under standard test conditions. An overall efficiency (η) of 2.94% is obtained with V_{OC} of 0.59 V and current density (J_{SC}) of 8.9 mA cm^{-2}.

To assess the stability of the device, we performed a 1000-hour test in air under constant illumination with no encapsulation applied to the device. IV scans were continually recorded every 0.5 h to characterize the V_{OC}, I_{SC}, *FF* and η. Between scans, the device was subjected to a 500 Ω resistive load. The lifetime testing apparatus is configured for mild aging conditions where a sulfur plasma lamp intensity delivers approximately 65–70 mW cm^{-2} and the substrate temperature is maintained at ~20 °C under ambient humidity. **Figure 2** shows normalized values for the photovoltaic parameters. Due to the slightly different spectral output and intensity of the sulfur lamp compared to the AM1.5G spectrum, we refer to Figure 1 for the starting values for each metric.

As can be seen in Figure 2, the cell experienced minor changes over the 1000-hour light soak. A slight decay in the V_{OC} and *FF* is observed which are offset by an increase in the I_{SC}. We speculate that the increase in the I_{SC} is likely due to

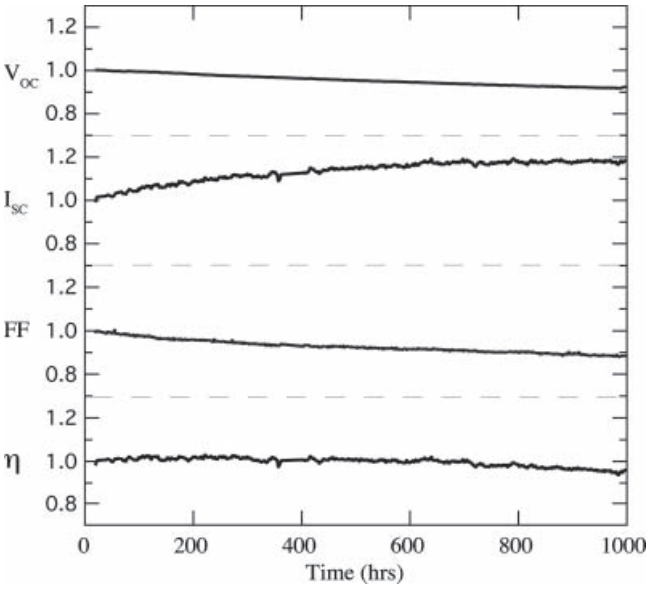

Figure 2. Device performance under constant illumination for 1000 h measured in air. IV scans are taken every 30 min for evaluation of each metric. The values are normalized on the unmasked device and we refer to Figure 1 for the initial values.

an increase in the conductivity of either the PbS film upon oxygen exposure,[10] an increase in the ZnO film from continual illumination,[17] or a decrease in the device resistance that may result from repetitive electrical measurement. This leads to a relatively unchanged device efficiency over the test period, which surpasses other PbX QD solar cells including those employing LiF as the electrode which degraded to near 87% of the initial efficiency after 63 h.[26] Upon concluding the 1000-hr test, the device was removed and the external quantum efficiency (EQE) was re-measured. **Figure 3** displays the spectral response of the solar cell before and after the 1000 hr test in air. Additionally we show the absorption spectrum for solutions of the starting ZnO and PbS NCs. The onset of absorption for ZnO occurs at 356 nm which is out of the active spectral region for the solar cell. The characteristic first exciton peak of 1.3 eV PbS at 950 nm is present in the extinction as well as the EQE, and did not blue-shift even after the air exposure test. In light of recent reports showing a dramatic shift in the first exciton with exposure to air,[15,28] a stable spectral response further suggests a lack of destructive oxidation occurring throughout this assessment. Our stability result also compares favorably to other solution processed PV technologies such as OPV.[29,30] Gur reported similar stability results after ~200 h using CdSe and CdTe NCs annealed into bulk-like films at 400 °C in selenium rich environments,[31] whereas the PbS film described here is not annealed and thus retains the favorable quantum confinement effects, such as a widened band gap. The widened band gap leads to a photovoltage greater than the bulk band gap of PbS, thus demonstrating suppressed recombination within the QD film with sufficient interQD electronic coupling needed for carrier transport in a quantum confined system.

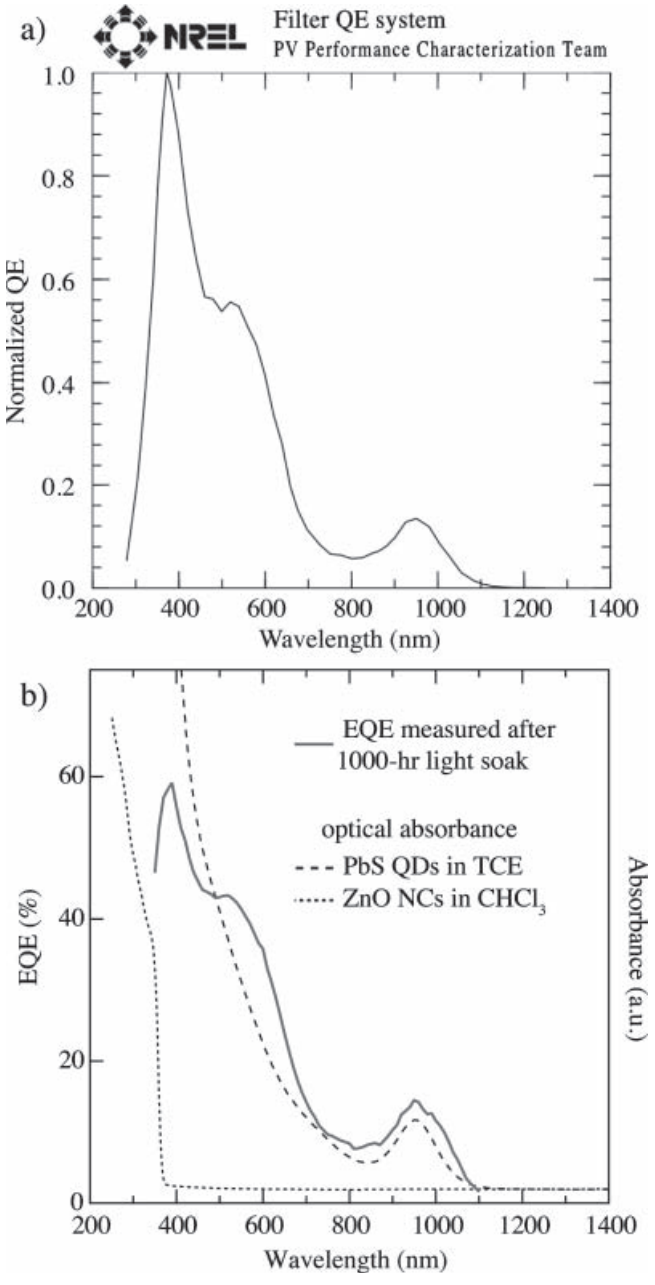

Figure 3. a) The normalized QE reported during the official measurement of the solar cell used for the calculation of the spectral mismatch. b) EQE spectrum of the device after the 1000-hour air stability assessment measured in our laboratory. The optical absorption of ZnO in chloroform and PbS in tetrachloroethylene is also shown for comparison. ZnO is transparent to wavelengths longer than 356 nm. The stable first exciton peak at 950 nm of the PbS QDs present in absorbance and the EQE of the device demonstrates the absence of destructive oxidation effects on the PbS film. The shoulder at 500–600 nm present in the EQE but not the optical absorbance is partially due to optical interference in the planar 70 nm PbS QD film.

Further gains in efficiency are possible in this architecture by employing larger band gap QDs to yield a higher V_{OC}, thicker PbS films to enhance J_{SC} and perhaps other *n*-type films below the QD layer. The performance demonstrated here represents a firm basis on which to compare future devices since this is the first QD solar cell with a certified 1-sun conversion efficiency. We demonstrate excellent stability in PbS QD-based solar cell for 1000 hours of continuous illumination in ambient air conditions.

Experimental Section

Materials: Zinc acetate ($ZnAc_2$, 99.99%, Sigma-Aldrich), potassium hydroxide (KOH, certified ACS pellets, Fisher Scientific), lead oxide (PbO, Puratronic, 99.9995%, Alfa Aesar), hexamethyldisilathiane (synthesis grade, Sigma-Aldrich), oleic acid (OA, tech. grade 90%, Sigma-Aldrich), 1-octadecene (ODE, tech. grade 90%, Sigma-Aldrich), 1,2-ethanedithiol (EDT, purum ≥98.0%, Fluka), chloroform (anhydrous, 99+%, Sigma-Aldrich), methanol (MeOH, anhydrous, 99.8%, Sigma-Aldrich), hexane (anhydrous, 95%, Sigma-Aldrich), ethanol (anhydrous, ≥99.5%), and acetonitrile (anhydrous, 99.8%, Sigma-Aldrich) were purchased and used as received.

Nanocrystal synthesis: Synthesis of ZnO NCs was carried out by adding $ZnAc_2$ (4.4 g) to MeOH (200 mL), heating to 60 °C and dropwise addition of a 0.4M KOH (100 mL) solution in MeOH. The solution was stirred at 60 °C for 2 h. The particles were extracted via centrifuge and re-suspended in MeOH. This was repeated three times, and finally the dry ZnO powder was moved into a glove box and dispersed in $CHCl_3$ (40 mL).

We synthesized PbS QDs with a first exciton peak at 950 nm (1.3 eV) by adding PbO (0.47 g), OA (2 g), and ODE (10 g) to a three-neck round bottom flask. This mixture was heated to 120 °C under vacuum for 2 h and then kept under N_2. In a glove box, hexamethyldisilathiane (180 µL) was mixed with ODE (5 mL) and loaded into a syringe. The contents

of the syringe were injected into the flask and 1 min later the heating mantle was removed and the QDs were cooled to room temperature. The reaction solution was mixed with hexane (10 mL) and ethanol (20 mL) and centrifuged to extract the QDs. Hexane and ethanol were used again for an additional purification step, and the QDs were then suspended in hexane with oleate molecules capping the QDs and stored in air or a N_2 desiccator until use.

Device fabrication: The ZnO nanoparticle solution was spin-coated at 2000 RPM for 1 min onto a cleaned glass substrate with prepatterned ITO electrodes (Thin Film Devices, Anaheim). The resulting ZnO film (100 nm thick) was annealed on a hotplate set to 260 °C for 30 min to remove residual solvent. A PbS QD film was deposited onto the ZnO film via dip coating described previously.[10] In this case, the PbS QD film was deposited by 20 iterations of sequentially immersing the substrate into PbS QDs in hexane (concentration 10 mg mL^{-1}) and then 1 mM EDT in acetonitrile in a fume hood. Gold was then evaporated onto the top of the film at a rate of 0.2 nm/sec and base pressure of 1×10^{-7} Torr. A device is formed with an active area of 0.11 cm^2 defined by the overlap of Au and ITO. A copper mask was then adhered onto the glass with a defined aperture of 0.0293 cm^2 to rule out the errors in device area often seen with small area solution deposited devices formed without accurate mesa etches.[32]

Acknowledgements

We thank Matt Law and Randy Ellingson for helpful suggestions. JML, OES, AJN were supported by the Center for Advanced Solar Photophysics, an Energy Frontier Research Center funded by US Department of Energy, Office of Science, Office of Basic Energy Sciences. MTL acknowledges funding from the National Center for Photovoltaics. JG and MCB acknowledge funding from the seed program of EERE of the Department of Energy. DOE funding was provided to NREL through contract DE-AC36–08GO28308.

Received: March 31, 2010
Published online: June 8, 2010

[1] F. W. Wise, *Acc. Chem. Res.* **2000**, *33*, 773.
[2] M. A. Hines, G. D. Scholes, *Adv. Mater.* **2003**, *15*, 1844.
[3] C. M. Evans, L. Guo, J. J. Peterson, S. Maccagnano-Zacher, T. D. Krauss, *Nano Lett.* **2008**, *8*, 2896.
[4] J. M. Pietryga, R. D. Schaller, D. Werder, M. H. Stewart, V. I. Klimov, J. A. Hollingsworth, *J. Am. Chem. Soc.* **2004**, *126*, 11752.
[5] M. V. Kovalenko, D. V. Talapin, M. A. Loi, F. Cordella, G. Hesser, M. I. Bodnarchuk, W. Heiss, *Angew. Chem. Int. Ed.* **2008**, *47*, 3029.
[6] D. V. Talapin, C. B. Murray, *Science* **2005**, *310*, 86.
[7] R. Y. Wang, J. P. Feser, J. S. Lee, D. V. Talapin, R. Segalman, A. Majumdar, *Nano Lett.* **2008**, *8*, 2283.
[8] G. Konstantatos, I. Howard, A. Fischer, S. Hoogland, J. Clifford, E. Klem, L. Levina, E. H. Sargent, *Nature* **2006**, *442*, 180.
[9] E. J. D. Klem, D. D. MacNeil, P. W. Cyr, L. Levina, E. H. Sargent, *Appl. Phys. Lett.* **2007**, *90*.
[10] J. M. Luther, M. Law, Q. Song, C. L. Perkins, M. C. Beard, A. J. Nozik, *ACS Nano* **2008**, *2*, 271.
[11] J. M. Luther, M. Law, M. C. Beard, Q. Song, M. O. Reese, R. J. Ellingson, A. J. Nozik, *Nano Lett.* **2008**, *8*, 3488.
[12] G. I. Koleilat, L. Levina, H. Shukla, S. H. Myrskog, S. Hinds, A. G. Pattantyus-Abraham, E. H. Sargent, *ACS Nano* **2008**, *2*, 833.
[13] W. Ma, J. M. Luther, H. M. Zheng, Y. Wu, A. P. Alivisatos, *Nano Lett.* **2009**, *9*, 1699.
[14] M. Law, J. M. Luther, Q. Song, B. K. Hughes, C. L. Perkins, A. J. Nozik, *J. Am. Chem. Soc.* **2008**, *130*, 5974.
[15] M. H. Zarghami, Y. Liu, M. Gibbs, E. Gebremichael, C. Webster, M. Law, *ACS Nano* **2010**, *4*, 2475.
[16] C. Wadia, A. P. Alivisatos, D. M. Kammen, *Environ: Sci. Technol.* **2009**, *43*, 2072.
[17] J. J. Choi, Y. F. Lim, M. B. Santiago-Berrios, M. Oh, B. R. Hyun, L. F. Sung, A. C. Bartnik, A. Goedhart, G. G. Malliaras, H. D. Abruña, F. W. Wise, T. Hanrath, *Nano Lett.* **2009**, *9*, 3749.
[18] K. S. Leschkies, T. J. Beatty, M. S. Kang, D. J. Norris, E. S. Aydil, *ACS Nano* **2009**, *3*, 3638.
[19] K. S. Leschkies, A. G. Jacobs, D. J. Norris, E. S. Aydil, *Appl. Phys. Lett.* **2009**, *95*.
[20] B. Sun, A. T. Findikoglu, M. Sykora, D. J. Werder, V. I. Klimov, *Nano Lett.* **2009**, *9*, 1235.
[21] S. W. Tsang, H. Fu, R. Wang, J. Lu, K. Yu, Y. Tao, *Appl. Phys. Lett.* **2009**, *95*.
[22] B.-R. Hyun, Y.-W. Zhong, A. C. Bartnik, L. Sun, H. D. Abruña, F. W. Wise, J. D. Goodreau, J. R. Matthews, T. M. Leslie, N. F. Borrelli, *ACS Nano* **2008**, *2*, 2206.
[23] M. S. White, D. C. Olson, S. E. Shaheen, N. Kopidakis, D. S. Ginley, *Appl. Phys. Lett.* **2006**, *89*.
[24] M. Law, M. C. Beard, S. Choi, J. M. Luther, M. C. Hanna, A. J. Nozik, *Nano Lett.* **2008**, *8*, 3904.
[25] J. Tang, L. Brzozowski, D. A. R. Barkhouse, X. H. Wang, R. Debnath, R. Wolowiec, E. Palmiano, L. Levina, A. G. Pattantyus-Abraham, D. Jamakosmanovic, E. H. Sargent, *ACS Nano* **2010**, *4*, 869.
[26] J. Tang, X. Wang, L. Brzozowski, D. A. R. Barkhouse, R. Debnath, L. Levina, E. H. Sargent, *Adv. Mater.* **2010**, *22*, 1398.
[27] V. Shrotriya, G. Li, Y. Yao, T. Moriarty, K. Emery, Y. Yang, *Adv. Funct. Mater.* **2006**, *16*, 2016.
[28] M. Sykora, A. Y. Koposov, J. A. McGuire, R. K. Schulze, O. Tretiak, J. M. Pietryga, V. I. Klimov, *ACS Nano* **2010**, *4*, 2021.
[29] B. Zimmermann, U. Wurfel, M. Niggemann, *Sol. Energy Mater. Sol. Cells* **2009**, *93*, 491.
[30] K. Lee, J. Y. Kim, S. H. Park, S. H. Kim, S. Cho, A. J. Heeger, *Adv. Mater.* **2007**, *19*, 2445.
[31] I. Gur, N. A. Fromer, M. L. Geier, A. P. Alivisatos, *Science* **2005**, *310*, 462.
[32] A. Cravino, P. Schilinsky, C. J. Brabec, *Adv. Funct. Mater.* **2007**, *17*, 3906.